J. Fluid Mech. (1966), *vol.* 25, *part* 2, *pp.* 337–366
Printed in Great Britain

The entrainment function in turbulent boundary-layer and wall-jet calculations

By M. P. ESCUDIER AND W. B. NICOLL

Imperial College of Science and Technology, Department of Mechanical Engineering, Exhibition Road, London, S.W. 7

(Received 30 September 1965)

Some of the proposals made by Spalding (1964*a*) in his 'Unified theory of friction, heat transfer, and mass transfer' are examined. The two-component velocity-profile family proposed by Spalding is compared with measured boundary-layer and wall-jet velocity profiles and is shown to be adequate for flows with moderate wake components. The drag law implicit in the velocity-profile family is shown to be in good agreement with experimental data.

Recommendations are provided for entrainment functions for both boundary layers and wall jets.

Predictions of boundary-layer and wall-jet development, based on the recommended entrainment functions, are presented and compared with experiment. The predictions are in good agreement with experiment except in the vicinity of separation.

1. Introduction

1.1. *Spalding's unified theory*

A general theoretical framework has been developed by Spalding (1964*a*) for the prediction of friction, heat transfer and mass transfer in turbulent boundary layers and wall jets. The calculation of the development of the hydrodynamic boundary layer† is based upon the ordinary differential equations for the integral conservation of mass and momentum and employs two auxiliary functions. These are:

(i) A two-parameter velocity profile having two components; one accounting for the effects of mass and momentum transfer to the wall, and the other for interactions with the mainstream.

(ii) A function which relates the rate of mass-entrainment by the boundary layer from the mainstream to the profile and flow parameters.

The utility of the theory depends upon the range of flows for which adequate auxiliary functions can be determined.

1.2. *Object of the present paper*

The present work has three main tasks. These are:

(i) To compare with experimental profiles the velocity profile proposed by Spalding (1964*a*).

† Unless otherwise stated, the term 'boundary layer' may be taken to include wall-jet flows.

(ii) To present the results of a survey of the experimental data which have been analysed for information about entrainment and to recommend entrainment functions for boundary layers and wall jets.

(iii) To compare with experiment the predictions of the 'unified theory', using the entrainment functions determined in (ii) above.

1.3. *Restrictions*

The restrictions to which the flows considered in the the present paper are subject are: (i) uniform fluid properties; (ii) hydrodynamically smooth wall; (iii) impermeable wall; (iv) two-dimensional flow.

2. Mathematical theory

The object of this section is to derive the equations used for the prediction of boundary-layer development and to illustrate the role of the velocity-profile and entrainment assumptions in the theoretical structure of the 'unified theory'.

The first of the two differential equations to be used is that expressing the integral conservation of mass in the boundary layer. This may be written as

$$\frac{d}{dx}\left(\int_0^{v_G} \rho u\, dy\right) = -\rho v_G + \rho u_G \frac{dy_G}{dx}, \tag{2.1}$$

where v_G is the velocity at the outer edge of the boundary layer normal to the surface, and y_G is the boundary-layer thickness. The right-hand side of equation (2.1) represents the total rate of entrainment of mass from the mainstream into the boundary layer. Equation (2.1) can be re-written

$$\frac{d}{dx}\left(\int_0^{v_G} \rho u\, dy\right) = -\dot{m}''_G, \tag{2.2}$$

where the entrainment rate $-\dot{m}''_G$ is defined as

$$-\dot{m}''_G \equiv -\rho v_G + \rho u_G\, dy_G/dx. \tag{2.3}$$

The other differential equation used is the von Kármán momentum integral equation,

$$\frac{d\delta_2}{dx} + (2+H)\frac{\delta_2}{u_G}\frac{du_G}{dx} = \tfrac{1}{2}c_f, \tag{2.4}$$

where δ_2 is the momentum thickness of the boundary layer, H the ratio of the displacement thickness δ_1 to the momentum thickness and $\frac{1}{2}c_f$ the local drag coefficient, defined by

$$\tfrac{1}{2}c_f \equiv \tau/(\rho u_G^2), \tag{2.5}$$

where τ is the local shear stress at the wall.

We follow Spalding (1964*a*) in defining the following non-dimensional quantities:

$$\mathrm{R}_m \equiv \int_0^{v_G} \frac{u}{\nu}\, dy, \qquad \mathrm{R}_x \equiv \int_0^{x} \frac{u_G}{\nu}\, dx, \tag{2.6), (2.7}$$

$$\mathrm{R}_2 \equiv u_G \delta_2/\nu, \qquad s \equiv \tfrac{1}{2}c_f, \tag{2.8), (2.9}$$

and

$$-m_G \equiv -\dot{m}''_G/(\rho u_G). \tag{2.10}$$

Equation (2.2) may then be re-written as

$$d\mathrm{R}_m/d\mathrm{R}_x = -m_G, \tag{2.11}$$

and equation (2.4) as

$$\frac{d\mathrm{R}_2}{d\mathrm{R}_x} + (1+H)\,\mathrm{R}_2 \frac{d(\ln u_G)}{d\mathrm{R}_x} = s. \tag{2.12}$$

Equations (2.11) and (2.12) would constitute a soluble set if all the quantities except R_x could be expressed as functions of any two (independent) dependent variables, either explicitly or implicitly through auxiliary relationships. We again follow Spalding in obtaining the required relationships through velocity-profile and entrainment assumptions.

The velocity profile is assumed to be a member of the two-parameter family

$$z = s^{\frac{1}{2}} f\{y^+\} + (1-z_E)\, g\{\xi\}, \tag{2.13}$$

where $z \equiv u/u_G$, $\xi \equiv y/y_G$ and $y^+ \equiv \sqrt{(\tau/\rho)}\, y/\nu$. The quantity z_E is a profile parameter and f and g are universal functions. The physical basis for this assumption and specific forms for f and g will be discussed in § 3. The boundary condition $\xi = 1 : z = 1$, together with the fact that $g\{\xi\}$ is so normalized that $g\{1\} = 1$, yields the local drag law

$$s^{\frac{1}{2}} = z_E/f\{y_G^+\} = z_E/f_G. \tag{2.14}$$

For a wall jet, where $z_E > 1$, the momentum-thickness Reynolds number R_2 passes through zero and the shape factor H through infinity. For the purposes of the numerical integration of equations (2.11) and (2.12), therefore, it is convenient to eliminate R_2 and H. To do this the quantities I_1 and I_2 are introduced, defined by

$$I_1 \equiv \int_0^1 z\, d\xi, \tag{2·15}$$

and

$$I_2 \equiv \int_0^1 z^2\, d\xi. \tag{2·16}$$

Then we have

$$\mathrm{R}_m = \mathrm{R}_2\left(1 - \frac{I_1}{I_2}\right), \qquad H = \frac{1-I_1}{I_1 - I_2}, \tag{2.17), (2.18}$$

and equation (2.12) may be written

$$\mathrm{R}_m \frac{d}{d\mathrm{R}_x}\left(\frac{I_2}{I_1}\right) = \left(\frac{1-I_2}{I_1}\right) \mathrm{R}_m \frac{d(\ln u_G)}{d\mathrm{R}_x} - s + \left(\frac{I_1 - I_2}{I_1}\right)(-m_G). \tag{2.19}$$

We can expand $d(I_2/I_1)/d\mathrm{R}_x$ as

$$\frac{d}{d\mathrm{R}_x}\left(\frac{I_2}{I_1}\right) = \frac{1}{I_1}\left(\frac{\partial I_2}{\partial z_E}\frac{dz_E}{d\mathrm{R}_x} + \frac{\partial I_2}{\partial f_G}\frac{df_G}{d\mathrm{R}_x}\right) - \frac{I_2}{I_1^2}\left(\frac{\partial I_1}{\partial z_E}\frac{dz_E}{d\mathrm{R}_x} + \frac{\partial I_2}{\partial f_G}\frac{df_G}{d\mathrm{R}_x}\right). \tag{2.20}$$

However, the quantity f_G which appears in the drag law and, through the drag law, in the expressions for I_1 and I_2 is found to be slowly varying, so the terms in equation (2.20) containing $df_G/d\mathrm{R}_x$ can be neglected. Equation (2.19) thus becomes, after some re-arrangement,

$$\mathrm{R}_m \frac{dz_E}{d\mathrm{R}_x} = \frac{(1-I_2)\,\mathrm{R}_m\, d(\ln u_G)/d\mathrm{R}_x - I_1 s + (I_1 - I_2)(-m_G)}{(\partial I_2/\partial z_E - I_2/I_1\, \partial I_1/\partial z_E)_{f_G}}. \tag{2.21}$$

With the exception of $-m_G$, all the quantities appearing in equations (2.11 and (2.21) may be related to the main dependent variables R_m and z_E. Thus, once the entrainment function $-m_G$ has been determined, the development of hydrodynamic boundary layers may be predicted, all that is required being the solution of two simultaneous, non-linear, ordinary differential equations.

3. Velocity profile

3.1. *Previous recommendations*

Coles (1956), after an extensive review of low-speed boundary-layer data, proposed the velocity profile

$$u^+ = f\{y^+\} + \frac{2\Pi}{\kappa} g\{\xi\}, \tag{3.1.1}$$

where both $f\{y^+\}$ and $g\{\xi\}$ are functions supposed common to all two-dimensional turbulent boundary layers, Π is a profile parameter and κ a constant. The function $f\{y^+\}$ is termed 'the law of the wall' and, following Coles, $g\{\xi\}$ 'the law of the wake'.

Experiment shows that the law of the wall has the form

$$f\{y^+\} = \frac{1}{\kappa} \ln (Ey^+), \tag{3.1.2}$$

where κ and E are constants. Coles (1956) recommended the values

$$\kappa = 0{\cdot}40, \quad E = 7{\cdot}691;$$

and later (1962)

$$\kappa = 0{\cdot}41, \quad E = 7{\cdot}768.$$

Chi (1962) found that boundary-layer drag data indicate

$$\kappa = 0{\cdot}40, \quad E = 12.$$

Other authors (e.g. Clauser 1954; Spalding 1964*a*, 1965; etc.) have recommended various other values for κ and E. The present authors have followed Spalding (1964*a*) in using

$$\kappa = 0{\cdot}40, \quad E = 6{\cdot}542.$$

Coles (1956) expressed his recommendation for the law of the wake in tabular form and, as was noted by Hinze (1959), this differs only slightly from

$$g\{\xi\} = \tfrac{1}{2}(1 - \cos \pi\xi). \tag{3.1.3}$$

Equation (3.1.3) is compared with Coles' $g\{\xi\}$ relation in figure 1.

Spalding (1964*a*, 1965) used a slightly different profile parameter from Coles' Π and wrote equation (3.1.1) as

$$u^+ = \frac{1}{\kappa} \ln (Ey^+) + (1 - z_E)\, \tfrac{1}{2}(1 - \cos \pi\xi)\, u_G^+, \tag{3.1.4}$$

where the specific forms mentioned above have been utilized for the wall and wake components. The profile parameter z_E can be interpreted physically as the ratio of the law-of-the-wall velocity at the outer edge of the boundary layer to the mainstream velocity. The quantity $(1 - z_E)$ is a measure of the relative magnitude

of the wake-component of the velocity profile. Typical wall and wake components and total velocity profiles are shown in figure 2 for $z_E < 1$ and $z_E > 1$.

Coles (1956), in his determination of the law of the wake, examined only 'conventional' boundary-layer profiles where $z_E < 1$, whereas Spalding (1964*a*) assumed that the same $g\{\xi\}$ function could be used for all boundary layers with $z_E > 0$, including wall-jet flows where $z_E > 1$. One of the aims of the present work

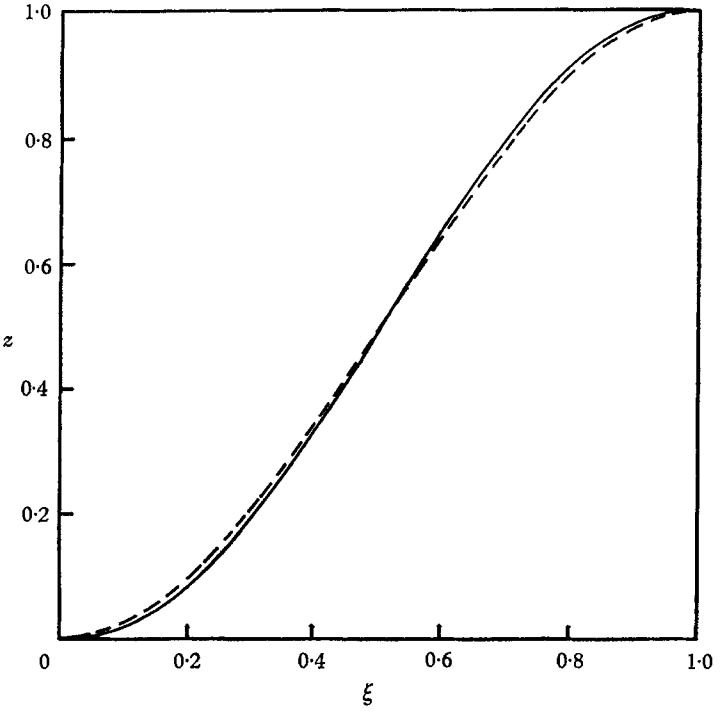

FIGURE 1. Comparison of $z = \frac{1}{2}(1-\cos \pi\xi)$ with Coles's law of the wake. ——, Coles's law of the wake; — — —, $z = \frac{1}{2}(1-\cos \pi\xi)$.

is to examine velocity profiles covering the whole range of z_E values to see if Spalding's assumption is justifiable. Coles himself noted that it was not possible to find satisfactory values for the parameters Π, u_τ ($\equiv \sqrt{(\tau/\rho)}$) and y_G such that equation (3.1.1) would fit a profile, measured by Klebanoff & Diehl (1952), downstream of a point of reattachment. Coles also remarked that experiments performed by Wieghardt (1944) indicated that there is a definite change in the shape, as well as in the amplitude, of the wake component in flow at constant pressure when the level of free-stream turbulence is varied.

3.2. *Drag law*

As shown in § 2, equation (3.1.1) implies a drag law. If we use the form for $f\{y^+\}$ given in equation (3.1.2), the drag law, equation (2.14), becomes

$$s = (\kappa z_E/l)^2, \tag{3.2.1}$$

where

$$l \equiv \ln(Ey_G^+) = \ln(E\mathrm{R}_G s^{\frac{1}{2}}). \tag{3.2.2}$$

It is worth pointing out, perhaps, that the drag law represented by equation (3.2.1) is independent of the specific form of the wake profile assumed.

The drag law deduced from the velocity profile adopted here is compared, in figure 3, with the proposal of Ludwieg & Tillmann (1949) that

$$s = 0{\cdot}123 \times 10^{-0{\cdot}678H} \mathrm{R}_2^{-0{\cdot}268}. \tag{3.2.3}$$

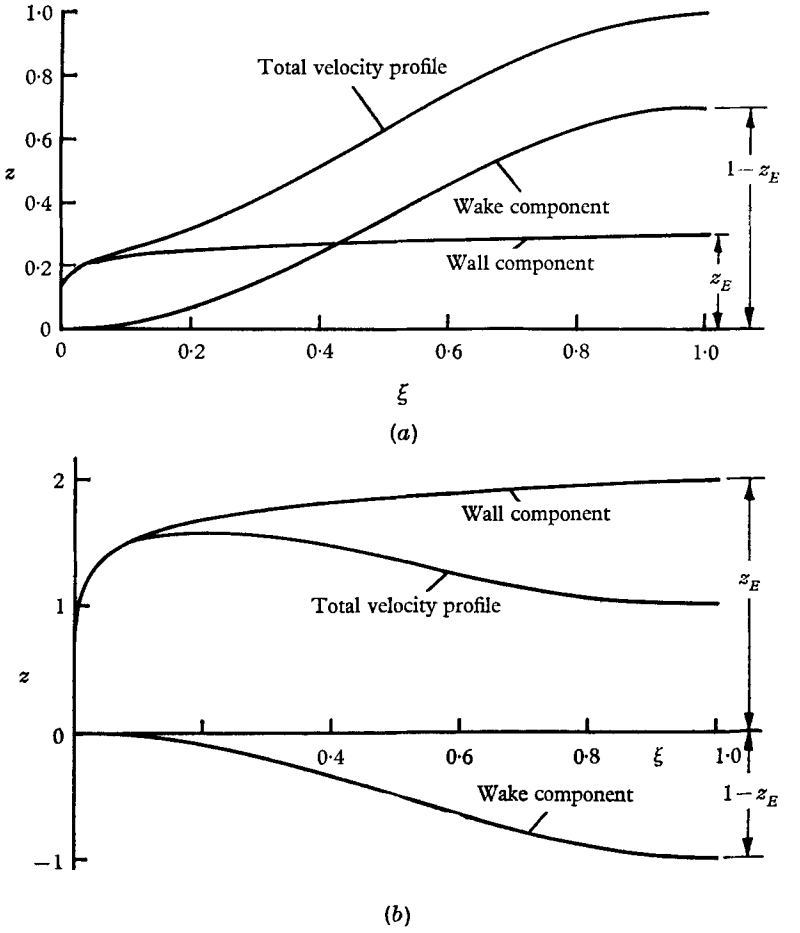

FIGURE 2. Typical velocity profiles according to equation (3.2.4). (*a*) Boundary-layer profile, $z_E < 1$. (*b*) Wall-jet profile, $z_E > 1$.

The present law clearly yields values for s which are lower than those given by equation (3.2.3); in this connexion it is worth mentioning that Newman (1951) showed the Ludwieg–Tillmann law to overestimate drag, particularly when H is large.

The present drag law is compared directly with experimental data in figure 4. There is considerable scatter, and it is seen that in many cases the wall shear stress is underestimated. Nevertheless, equation (3.2.1) is an improvement on the Ludwieg–Tillmann law for large H values and is the only available drag law which has been recommended for both wall jets and boundary layers. It will be retained, therefore, until a better law becomes available.

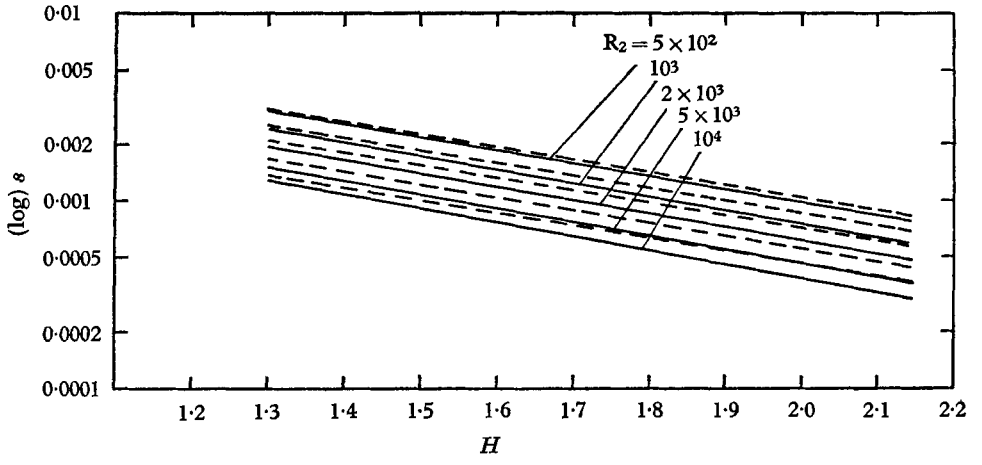

FIGURE 3. Comparison of drag law of Ludwieg & Tillmann (1949) with that derived from the velocity-profile equation (3.2.4). — — —, Ludwieg & Tillmann.

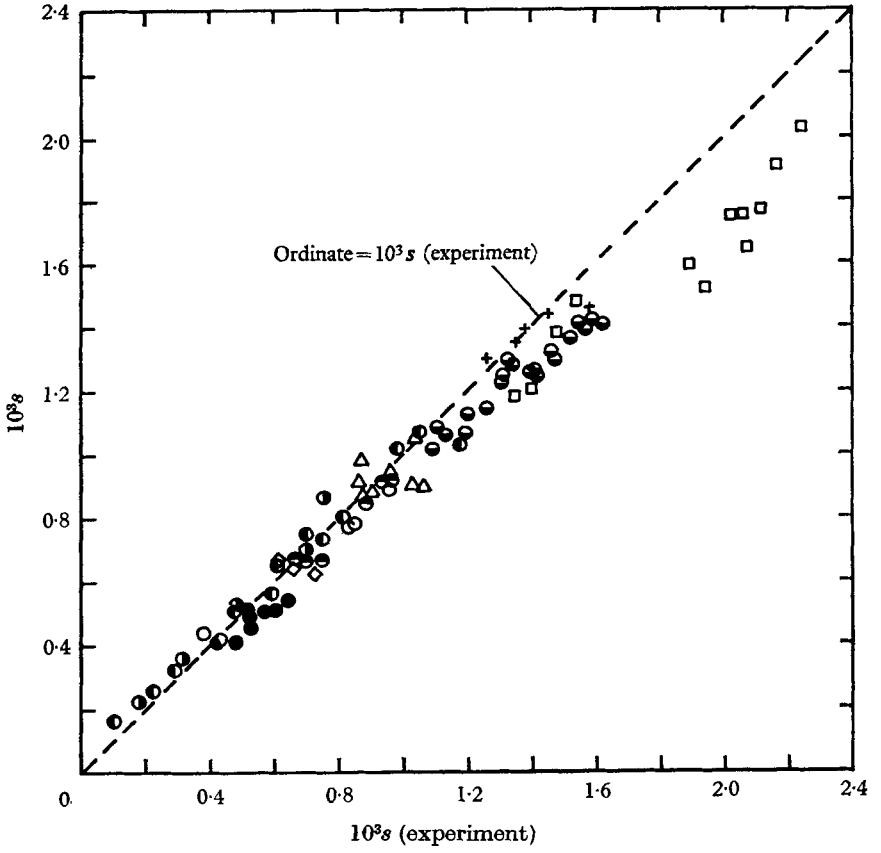

FIGURE 4. Drag coefficients computed from R_2 and H using present drag law compared with experimental data. ◒, Smith & Walker; +, Schultz-Grunow; ◓, recovering layer, ◇, equilibrium layer, Bradshaw & Ferriss; □, Fage & Falkner and Fage; ◐, Schubauer & Klebanoff; ◑, Newman; △, run 1, ●, run 2, Clauser.

Substitution of equation (3.2.1) into the definitions of u^+ and y^+ and substitution of the latter into equation (3.1.4) yields a form of the velocity profile more convenient for later work, it is

$$z = z_E[1 + (\ln \xi/l)] + (1 - z_E)\tfrac{1}{2}(1 - \cos \pi\xi). \tag{3.2.4}$$

3.3. *Comparison with experiment*

Values of the profile parameters have been determined for a number of experimental velocity profiles by the method of least-squares fitting. This procedure gives the values of z_E and y_G which minimize the square deviation R, defined by

$$R \equiv \sum_i [z\{y_i\} - z_i]^2,$$

z_i being the experimental velocity ratio at y_i, and $z\{y_i\}$ the value given by equation (3.2.4) at y_i. The measured and fitted profiles are shown in figures 5–11.

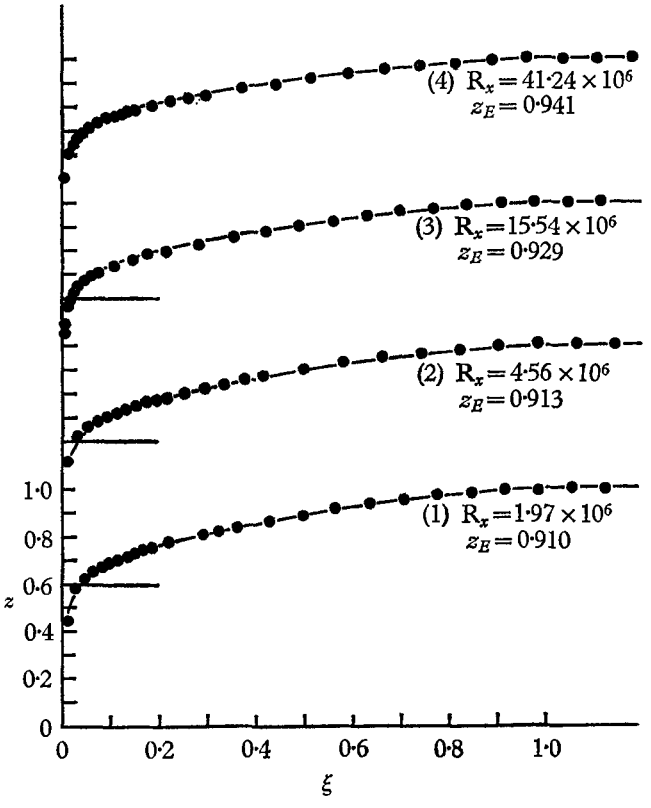

FIGURE 5. Comparison of equation (3.2.4) with experimental velocity profiles Smith & Walker (1959) for flat-plate boundary layers.

In figure 5, four profiles measured by Smith & Walker (1959) in boundary layers developing along a smooth, flat plate under zero pressure gradient are shown. The fitted profiles are evidently fairly good representations of the measured ones, although there is evidence of a small, but systematic, deviation from the fitted profile in the region of $\xi = 0{\cdot}3$. Values of the shape factor H

calculated from the fitted profiles differ by up to 4 % from the reported experimental values.

Similar remarks to those in the preceding paragraph can be made about the profiles of Bradshaw & Ferriss (1965) shown in figure 6. These data were obtained for a boundary layer recovering from the effects of an adverse pressure gradient—hence the relatively large wake-component at $x = 47$ in., where $z_E \approx 0{\cdot}67$.

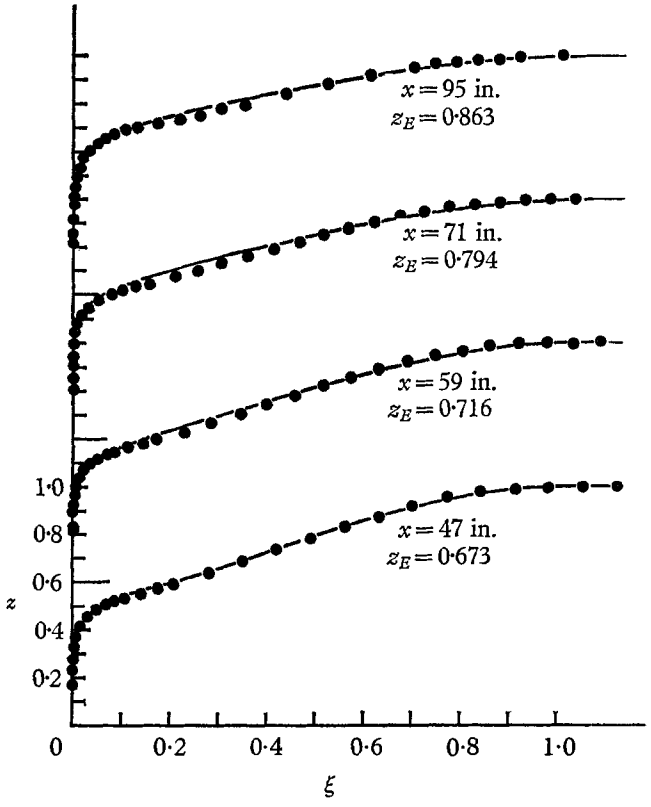

FIGURE 6. Comparison of equation (3.2.4) with experimental velocity profiles of Bradshaw & Ferriss (1965) for a boundary layer recovering from the effects of an adverse pressure gradient.

A purely cursory examination would indicate that equation (3.2.4) is a poorer fit to these data than to those of Smith & Walker, yet in this case the maximum difference between the reported experimental and computed values of H is less than 3 %. Clearly, careful thought must be given to deciding what constitutes 'a good fit'.

The profiles of Schubauer & Klebanoff (1951), shown in figure 7, were obtained for a boundary layer subjected to an adverse pressure gradient which eventually caused the layer to separate (a little beyond $x = 25$ ft.) Here again the profiles *appear* to be reasonably well-fitted by equation (3.2.4), although for the two downstream profiles shown, the theoretical profile is inadequate near the wall. The profile at $x = 25$ ft. has a large wake-component, the value of z_E being about

0·29, and in this case the shape factor calculated from the fitted profile is about 2·38, compared with the reported experimental value of 1·99.

The final set of velocity profiles for $z_E < 1$ are those of Stratford (1959), obtained for a boundary layer reported as having zero wall shear. In this case $z_E = 0$ and equation (3.2.4) reduces to the pure wake form

$$z = \tfrac{1}{2}(1 - \cos \pi\xi).$$

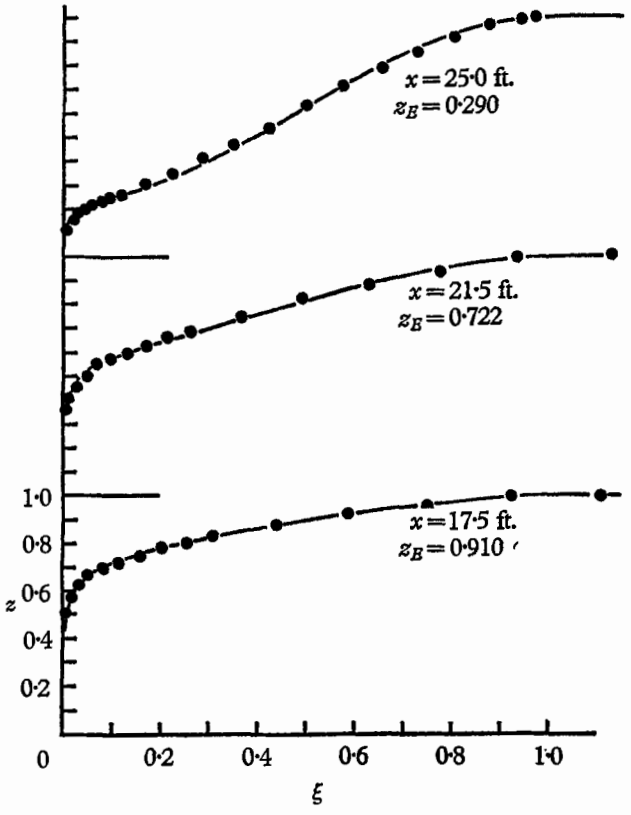

FIGURE 7. Comparison of equation (3.2.4) with experimental velocity profiles of Schubauer & Klebanoff (1951) for a boundary layer with an adverse pressure gradient.

It is seen, in figure 8, that this expression is a very poor representation of Stratford's data. Also, for $z_E = 0$, our profile gives the unique result $H = 4$, whereas Stratford's experiments gave values for H which varied from about 1·8 to 2·6.

All the cases considered above related to boundary layers with $1 > z_E \geqslant 0$. The remaining profiles, shown in figures 9–11, were obtained for boundary layers where $z_E > 1$, that is, for wall-jet flows. In all these cases the assumed profile deviates from the measured one in the same way, being too low near the edge of the layer and near the wall, and too high in the middle of the layer. The deviations are seen to increase in magnitude as z_E increases, that is, as the wake component becomes dominant. Also, the assumed profile gives roughly the correct value for the velocity maximum, but this always occurs further from the wall than the measured maximum.

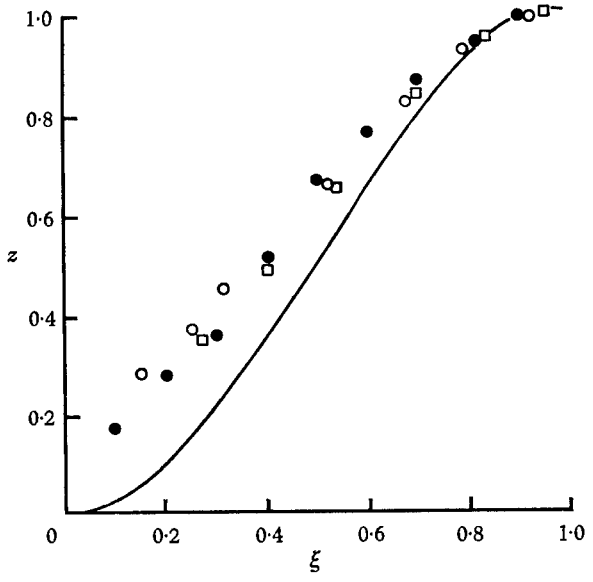

FIGURE 8. Comparison of $z = \frac{1}{2}(1-\cos\pi\xi)$ with experimental velocity profiles of Stratford (1959) for boundary layers with zero wall-shear stress.

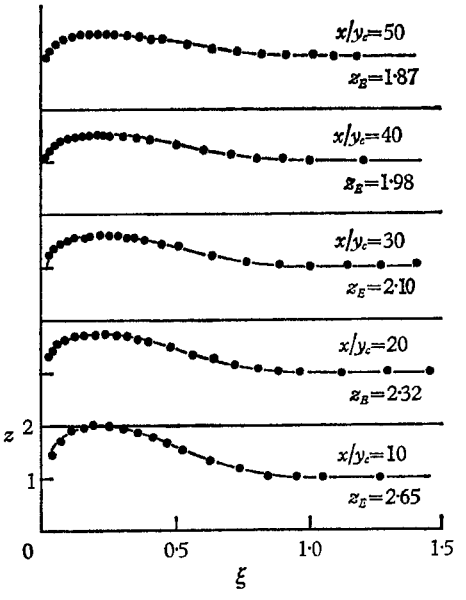

FIGURE 9. Comparison of equation (3.2.4) with experimental wall-jet velocity profiles of Nicoll (1965).

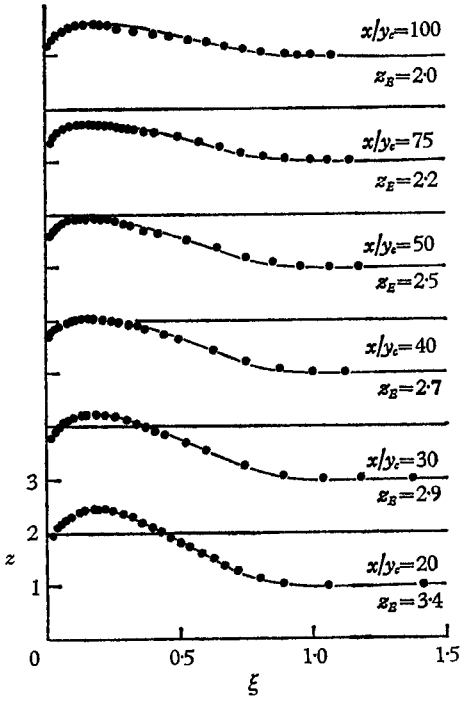

FIGURE 10. Comparison of equation (3.2.4) with experimental wall-jet velocity profiles of Nicoll (1965).

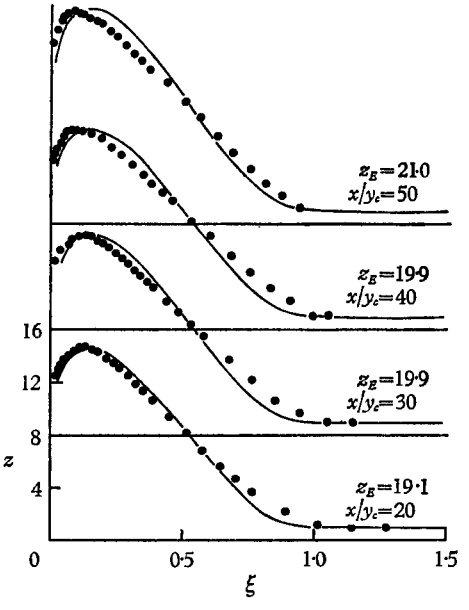

FIGURE 11. Comparison of equation (3.2.4) with experimental wall-jet velocity profiles of Nicoll (1965).

Clearly, for both $z_E > 1$ and $z_E < 1$ there is a need for improvement in the assumed velocity profile. The most obvious deficiency is probably the absence of a term to account for the effects of pressure gradient; current work is aimed at remedying this. For the time being, however, equation (3.2.4) will be retained as the velocity-profile assumption.

4. Entrainment function

4.1. *Review of previous recommendations*

The idea of using an entrainment function as the auxiliary equation in turbulent-boundary-layer calculations came from Head (1960). Head's entrainment function may be written, formally, as

$$-m_G = -m_G\{H_1\}, \tag{4.1.1}$$

where H_1 is a shape factor of the velocity profile, defined by

$$H_1 \equiv (y_G - \delta_1)/\delta_2 \tag{4.1.2}$$

(in terms of I_1 and I_2, $H_1 = I_1/(I_1 - I_2)$). Head made no recommendation for a velocity-profile family and therefore required, in addition to his entrainment function, a relation between the shape factors H and H_1 and also a drag law. The $H \sim H_1$ relation was deduced from experimental data, and the drag law assumed was that proposed by Ludwieg & Tillmann (1949). Head carried out calculations on a number of boundary layers and, in spite of his entrainment law being based upon only two sets of experimental data, those of Newman (1951) and Schubauer & Klebanoff (1951), obtained fairly satisfactory agreement with experiment. In all the cases considered, Head used the measured values of δ_2 in his calculations of H instead of calculating simultaneously δ_2 and H. Only in the case of the experiment of Newman was there poor agreement between the predicted and measured H values. This comparison was improved when δ_2 and H were simultaneously predicted.

Head's entrainment law is shown in figure 12.

The only other author to make recommendations for the entrainment function is Spalding (1964*a*, *b*, 1965). Spalding's first proposal (1964*a*) was

$$\left.\begin{aligned} z_E \leqslant 1: \quad & -m_G = 0{\cdot}1023(1 - z_E)\,(1 + \tfrac{1}{3}z_E), \\ z_E > 1: \quad & -m_G = 0{\cdot}09(z_E - 1)\,(1 + \tfrac{1}{3}z_E)/(1 + z_E). \end{aligned}\right\} \tag{4.1.3}$$

The basic form for these relations was arrived at by consideration of information relating to free mixing layers. The constants were determined from analyses of the equilibrium flat-plate boundary layer and of the spread and velocity-decay information available for wall jets.

In an annotated version of the paper cited above, Spalding (1964*b*) noted that equations (4.1.3) considerably over-estimate entrainment rates and remarked that these relations were over-elaborate. The following, simpler, relations were then proposed

$$\left.\begin{aligned} z_E \leqslant 1: \quad & -m_G = 0{\cdot}06(1 - z_E), \\ z_E > 1: \quad & -m_G = 0{\cdot}03(z_E - 1). \end{aligned}\right\} \tag{4.1.4}$$

The entrainment function was modified further in a more recent paper, Spalding (1965), to

$$\left.\begin{aligned} z_E \leqslant 1\text{:} \quad & -m_G = 0{\cdot}06 - 0{\cdot}05 z_E, \\ z_E > 1\text{:} \quad & -m_G = 0{\cdot}03 z_E - 0{\cdot}02. \end{aligned}\right\} \tag{4.1.5}$$

In figure 12 curves of $-m_G$ plotted against H_1, are drawn representing the proposals of Head (1960), of Spalding (1964*a*, *b*, 1965) and of the present authors, for the entrainment function for $z_E \leqslant 1$.

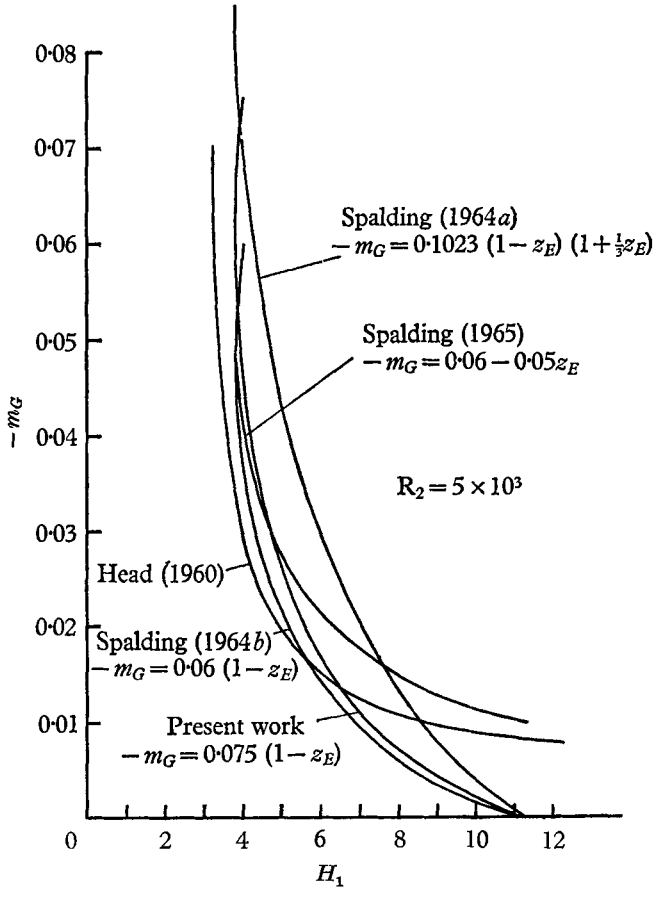

FIGURE 12. Comparison of various recommendations for the entrainment function for $z_E < 1$.

An entrainment law can be deduced from the hypothesis of Mellor & Gibson (1963) that the effective kinematic viscosity in the wake region of a boundary layer is equal to a constant times $u_G.\delta_1$ (the value of the constant was taken as 0·016). It is

$$z_E \leqslant 1\text{:} \quad -m_G \approx 0{\cdot}07(1-z_E). \tag{4.1.6}$$

This is not far different from Spalding's proposal, equation (4.1.4).

4.2. *Determination of entrainment rates from experimental data*

The basic information required in the determination of entrainment rates is the variation of R_m with R_x ,the value of $-m_G$ being determined by differentiation of R_m with respect to R_x. To deduce R_m from experimental velocity-profile data, it is necessary first to know the boundary-layer thickness y_G and it is evidently desirable to use a consistent method for determining this somewhat arbitrarily-defined quantity. One such method is to adopt a velocity-profile family, such as that represented by equation (3.2.4), and to determine the values of the profile-parameters which give the best fit to the experimental profile. Alternatively, properties of experimental velocity profiles, such as R_2 and H, can be matched with those given by the adopted profile and the profile-parameters determined in this way. With only a few exceptions, the data for wall jets ($z_E > 1$) and boundary layers ($z_E < 1$) have been analysed by different methods. The reasons for this are outlined below and the procedures then described.

One of the authors (W. B. N.) has been concerned exclusively with boundary layers where $z_E > 1$, and the other with flows for which $z_E < 1$. In the latter case, all the data examined were extracted from the literature, whereas many of the wall-jet data were obtained (by W. B. N.) in the authors' own laboratory. Experimental data are almost invariably published in the form of small-scale graphs and the retrieval of complete velocity-profile data is usually extremely difficult and time consuming. For this reason it was felt that, so far as boundary layers with $z_E < 1$ were concerned, best use could be made of the time available by deducing the profile parameters from integral properties of the velocity profiles. For wall jets, of course, most of the experimental data were at hand and, in the main, actual profiles could be analysed.

Naturally, the methods of analysis are complementary and, if the theoretical profile is a good representation of measured profiles, only small differences should arise in the final results.

4.2.1. *Analysis generally used for boundary-layer data where $z_E < 1$*

The velocity-profile expression assumed was that represented by equation (3.2.4). This is a two-parameter profile, so the parameters z_E and y_G, and all quantities associated with velocity profiles, such as R_m, R_G, H, s, etc., can be deduced from any two independent properties of a measured profile, together with the appropriate fluid properties (ρ and μ) and the mainstream velocity u_G.

The two quantities most commonly reported by boundary-layer experimenters are the momentum thickness δ_2 and shape factor H. These were the quantities from which most of the information concerning boundary layers was deduced. A computer program was developed to perform the computations and data from over five hundred profiles were analysed.

4.2.2. *Analysis generally used for wall-jet data*

The velocity profile adopted was again that represented by equation (3.2.1) and the fitting procedure the least-squares method described in § 3.3.

4.2.3. *Analysis occasionally used for wall-jet data*

When the detailed information required for the least-squares-fitting procedure was not available, the profile parameters were determined from the reported experimental values of $z_{\max}$ and $y_{\frac{1}{2}}$, where $z_{\max}$ is defined as the ratio of the maximum velocity in the wall jet to the mainstream velocity, and $y_{\frac{1}{2}}$ is the value of y at which $z = z_{\frac{1}{2}} = \frac{1}{2}(z_{\max}+1)$.

It may be seen from figures 9 to 11 that the least-squares-fitting procedure results in values for $z_{\max}$ and $y_{\frac{1}{2}}$ which agree well with the experimental values.

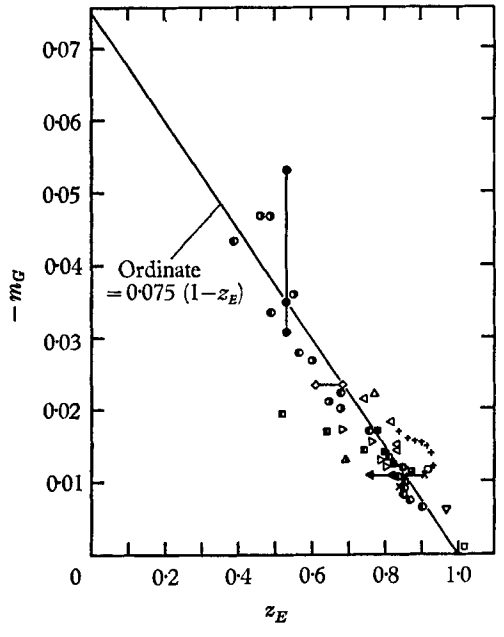

FIGURE 13

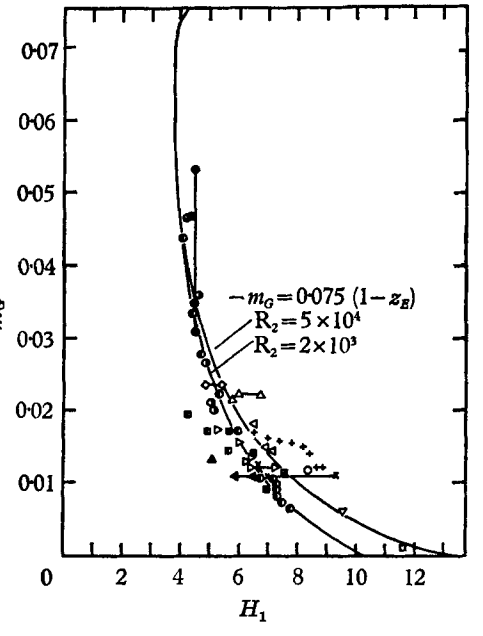

FIGURE 14

FIGURE 13. Entrainment rates deduced from experimental data for $z_E < 1$. ◪, Reynolds, Kays & Kline; ×, Smith & Walker; +, Schultz-Grunow, ○, Klebanoff; ◧ ◁ ◀ ▲ ■ ▷, Klebanoff & Diehl; △ run 1, ● run 2, Clauser; ◇, Bradshaw & Ferriss; ▽ □, Herring & Norbury; ◑, Newman; ◐, Schubauer & Klebanoff.

FIGURE 14. Entrainment rates deduced from experimental data for $z_E < 1$ plotted against Head's shape factor. Symbols as for figure 13.

4.3. *Discussion of entrainment data*

One of the attractive features of the entrainment function lies in the availability of data from which information about it can be obtained. A complete survey of velocity-profile data, of course, would be impossible, and in the present work a certain amount of selection has been necessary. An attempt has been made to include those data which are the most completely reported and, in the opinion of the present authors, the most reliable.

Entrainment rates deduced from all the data considered for boundary layers with $z_E < 1$ have been plotted against z_E and H_1 in figures 13 and 14 respectively.

Although the plot of $-m_G$ against z_E shows considerable scatter, the bulk of the data lends some support to an entrainment law of the form

$$-m_G = \text{const.}\,(1-z_E). \tag{4.3.1}$$

As was mentioned earlier, such a form was proposed by Spalding (1964*b*), the value for the constant being given as 0·06. The present investigation indicates 0·075 to be a better value, i.e.

$$-m_G = 0{\cdot}075(1-z_E). \tag{4.3.2}$$

This result is close to that deducible from the work of Mellor & Gibson (1963) (see § 4.1) and is the present authors' recommendation for $z_E < 1$.

Unfortunately, however, the data obtained for flat-plate boundary layers are irreconcilable with equation (4.3.2). The value of z_E appropriate to such boundary layers is about 0·92 and the corresponding value of $-m_G$, according to equation (4.3.2), is 0·006. The data of Klebanoff (1955), Reynolds, Kays & Kline (1958), Schultz-Grunow (1940) and Smith & Walker (1959) indicate $-m_G \approx 0{\cdot}011$, a value almost double that given above. The value of the constant in equation (4.3.1) would have to be 0·1375 to give $-m_G = 0{\cdot}011$ for $z_E = 0{\cdot}92$, and this would conflict with the data for $z_E < 0{\cdot}92$. This suggests that equation (4.3.1) may not be the best form for an entrainment function and perhaps indicates why Spalding (1965) was lead to propose the relation

$$-m_G = 0{\cdot}06 - 0{\cdot}05 z_E,$$

which gives $-m_G = 0{\cdot}014$ for $z_E = 0{\cdot}92$, a value more in keeping with the flat-plate data. Even so, this equation considerably overestimates entrainment rates for other boundary layers where $z_E \approx 0{\cdot}9$. It is not clear whether this apparent discrepancy in the data is due to scatter, which results from the difficulty of determining $-m_G$, or to the effect of some parameter, other than z_E, which influences the entrainment process.

The $-m_G \sim H_1$ plot in figure 14 shows that the assumption made by Head (1960), that $-m_G$ could be taken as a function of H_1 alone, was quite a reasonable one. Indeed the data so far examined show that the hypothesis of Spalding and of the present authors, that $-m_G = -m_G\{z_E\}$, is only a little better than Head's.

The entrainment data for $z_E > 1$ are shown in figure 15. As for $z_E < 1$, the data display considerable scatter, again probably due to the method of determination of $-m_G$ rather than to any real physical effect. This view is supported by the comparisons of predicted with experimental wall-jet development given in § 5.

The straight line shown in figure 15 represents the equation

$$-m_G = 0{\cdot}03 z_E - 0{\cdot}02, \tag{4.3.3}$$

and is the present authors' recommended entrainment relation for $z_E > 1$.

4.4. *Entrainment function for equilibrium flows*

For an equilibrium boundary layer, Spalding (1964*a*) intimated that the parameter z_E is nearly constant. For such flows, therefore, $dz_E/d\mathrm{R}_x$ can be regarded as negligible and equation (2.21) reduces to

$$(1-I_2)\,\mathrm{R}_m \frac{d(\ln u_G)}{d\mathrm{R}_x} - I_1 s + (I_1 - I_2)(-m_G) = 0. \tag{4.4.1}$$

We follow Clauser (1954, 1956) in defining a pressure-gradient parameter β:

$$\beta \equiv \frac{\delta_1}{\tau}\frac{dp}{dx} = -\frac{\mathrm{R}_1}{s}\frac{d(\ln u_G)}{d\mathrm{R}_x}, \tag{4.4.2}$$

which, as Clauser observed, should be constant for equilibrium flows. Equation (4.4.1) may then be re-arranged as

$$-m_G = H_1 s[1+\beta(1+1/H)], \tag{4.4.3}$$

where $H_1 \equiv (y_G-\delta_1)/\delta_2 = I_1/(I_1-I_2)$,

and $H \equiv \delta_1/\delta_2 = (1-I_1)/(I_1-I_2)$.

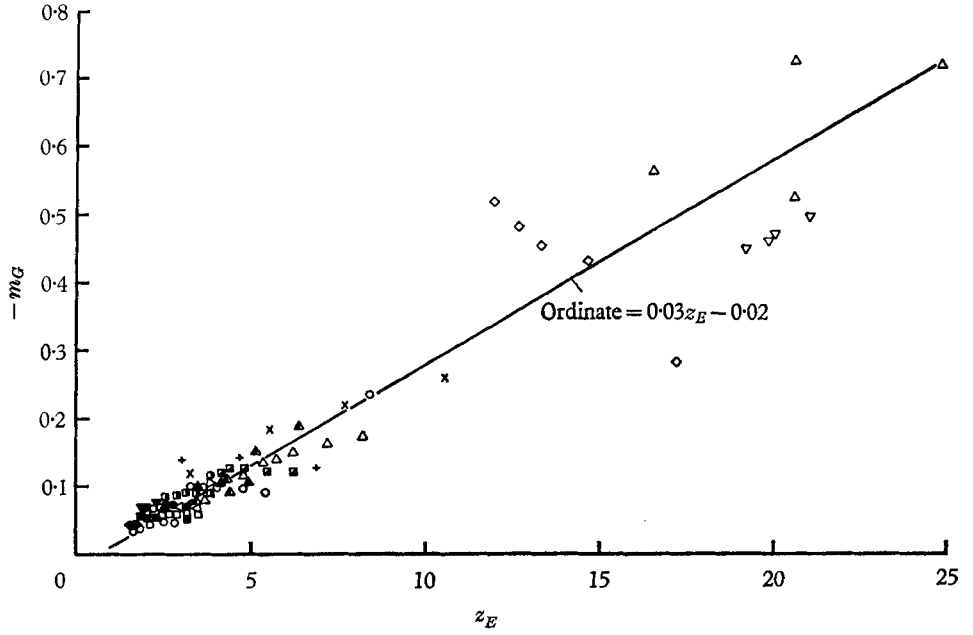

FIGURE 15. Entrainment rates deduced from experimental data for $z_E > 1$. ◁ ▲, Gartshore; ● ▲, Kruka & Eskinazi; ○ ◆ ■ ▼ □ △ ▽ ◇ ◪ ◨, Nicol; ▷ ◑, Patel & Newman; + ×, Seban & Back.

Clauser also showed that an appropriate shape factor for equilibrium flows is G, where

$$G \equiv \left(\int_0^1 F^2\,d\xi\right)\Big/\left(\int_0^1 F\,d\xi\right), \tag{4.4.4}$$

and $$F = (u_G-u)/u_\tau, \quad \text{the velocity defect.} \tag{4.4.5}$$

For a particular value of β, the velocity-defect profiles are independent of Reynolds number and therefore G is constant. Thus, for equilibrium boundary layers, there must be a unique relation between G and β. An empirical relation proposed by Nash (1965) for boundary layers with $z_E < 1$ is

$$G = 6{\cdot}1(\beta+1{\cdot}81)^{\frac{1}{2}} - 1{\cdot}7. \tag{4.4.6}$$

The parameter G is related to the more usual shape factor (H) as follows:

$$G = s^{-\frac{1}{2}}(1-1/H), \tag{4.4.7}$$

$$[\text{or} \quad G = s^{-\frac{1}{2}}(1-2I_1+I_2)/(1-I_1)].$$

Equations (4.4.3), (4.4.6), (4.4.7) and the velocity-profile assumption have been used to determine the curves of $-m_G$ against z_E plotted in figure 16. These curves again indicate that the effects of Reynolds number, measured through the parameter l, are comparatively unimportant and that the hypothesis $-m_G = -m_G\{z_E\}$ is a reasonable one. The curves clearly show the same trends as the experimental data and, perhaps, suggest that the data for flat-plate flows, flows with $z_E \to 0$ and flows with $z_E \approx 1$ will not be well represented by a single straight line (see § 4.3).

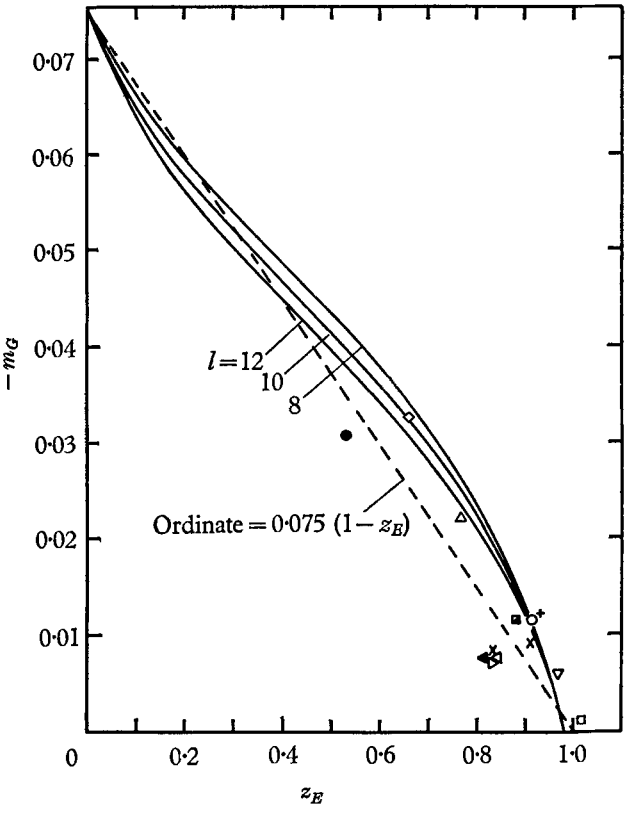

FIGURE 16. Comparison of theoretical entrainment rates for equilibrium boundary layers with experimental data. Symbols as for figure 13.

An interesting result deducible from the equilibrium-boundary-layer analysis is the value of $-m_G$ for $z_E = 0$. In this case, $s = 0$, $\beta = \infty$ and Nash's relation gives

$$G/\beta^{\frac{1}{2}} = 6{\cdot}1. \tag{4.4.8}$$

(N.B. Mellor & Gibson (1963) gave $G/\beta^{\frac{1}{2}} \to 5{\cdot}9$ for $\beta \to \infty$.) Thus, from equation (4.4.6)

$$\beta s = [1/(6{\cdot}1)^2](1 - 1/H)^2$$

and, from equation (4.4.3)

$$-m_G = H_1(\beta s)(1 + 1/H),$$

i.e.

$$-m_G = [H_1/(6{\cdot}1)^2](1 - 1/H)^2(1 + 1/H). \tag{4.4.9}$$

The assumed velocity profile then gives $z_E = 0$: $H = 4$, $H_1 = 4$, and equation (4.4.9) $-m_G = 0{\cdot}0756$. This result is in excellent agreement with the value for $-m_G$ obtained by extrapolation of the experimental data to $z_E = 0$.

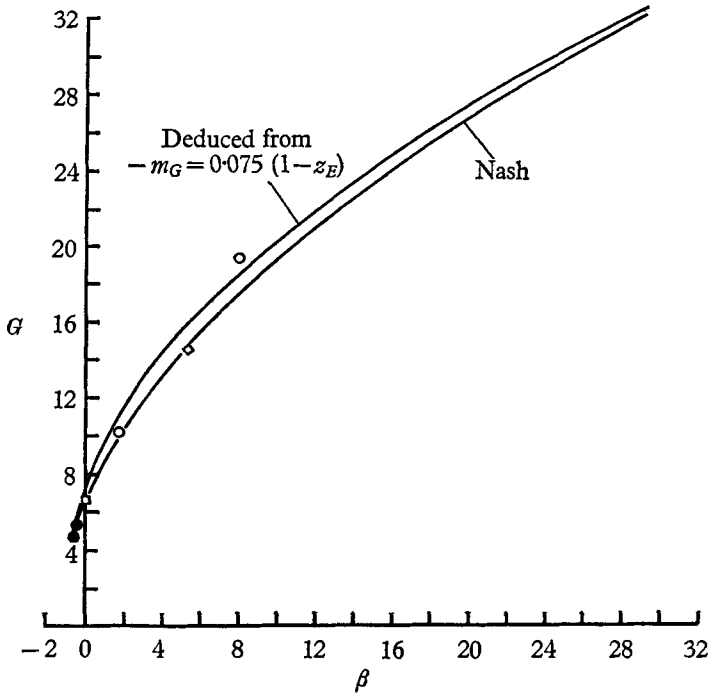

FIGURE 17. Comparison of the $G \sim \beta$ relation of Nash (1965) with the relation deduced from the entrainment function for $z_E < 1$ and with experimental data for equilibrium boundary layers. ●, Favourable pressure gradient, Herring & Norbury; □, zero pressure gradient, Klebanoff; ○, adverse pressure gradient, Clauser; ◇, adverse pressure gradient, Bradshaw & Ferriss.

The equilibrium analysis cannot, at present, be applied to wall-jet flows because Nash's $G \sim \beta$ relation is not valid for such flows. It is of some interest, however, to perform the inverse analysis and determine $G \sim \beta$ relations from the recommended entrainment functions for $z_E < 1$ and $z_E > 1$. The results of this analysis for $z_E < 1$ are shown in figure 17 together with Nash's relation and the available experimental data. The curves for $l = 8$, 10 and 12 are indistinguishable, and the differences between the curves deduced from $-m_G = 0{\cdot}075(1-z_E)$ and Nash's formula are slight. Although the available experimental data for equilibrium boundary layers are sparse, it would seem that there is little to choose between Nash's formula and a $G \sim \beta$ relation deduced via the entrainment function. Also, an entrainment function based upon a $G \sim \beta$ relation is clearly sensitive to the relation adopted.

For equilibrium wall jets, the $G \sim \beta$ relation implied by the entrainment law $-m_G = 0{\cdot}03z_E - 0{\cdot}02$ is shown in figure 18. The practical limitations of experimental apparatus limit accessible values of l to the vicinity of 10 and the spread

with l is thus rather unrealistic (to change l by 10% would require a change of roughly 250% in R_G). The experimental data of Patel & Newman (1961) are shown in figure 18 and are consistent with the $G \sim \beta$ relation deduced for $l = 10$.

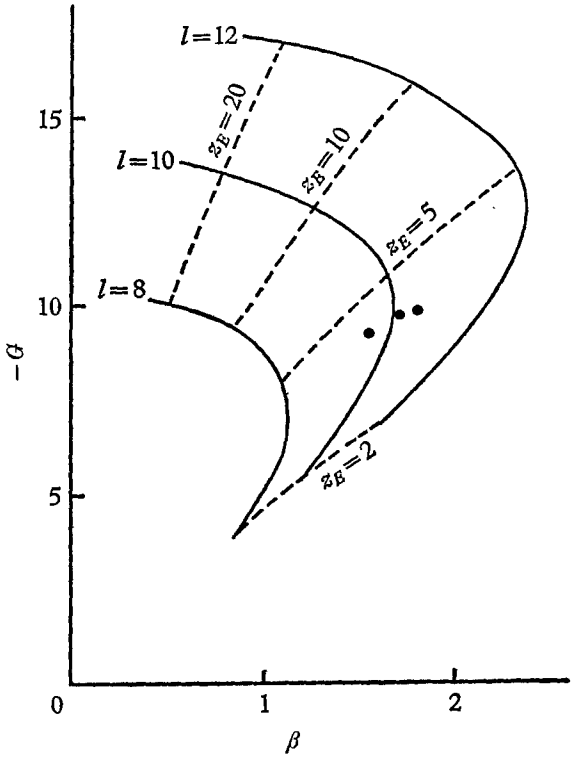

FIGURE 18. The $G \sim \beta$ relation for equilibrium wall jets deduced from the entrainment function for $z_E > 1$. ●, Patel & Newman.

4.5. *Conclusions and recommendations regarding the entrainment function*

The main obstacle in the determination of entrainment rates is the difficulty of specifying the boundary-layer thickness. To a certain extent this has been overcome and some degree of consistency achieved by adopting a velocity-profile family, the thickness and other profile-parameters being determined by fitting this to the experimental profiles or quantities derived from the profiles.

Analysis of a large amount of data has indicated that the hypothesis

$$-m_G = -m_G\{z_E\}$$

is a little better than that of Head (1960), $-m_G = -m_G\{H_1\}$, although there is considerable scatter in both the $-m_G \sim z_E$ and $-m_G \sim H_1$ plots. The difficulties and inherent inaccuracies involved in the determination of $-m_G$ preclude the inclusion of parameters other than z_E in an entrainment function, although the possible importance of other parameters (such as l, $dz_E/d\mathrm{R}_x$, etc.) cannot be ruled out.

The following entrainment functions appear to fit the experimental data as well as any; they will be used, for the time being at least, as auxiliary equations in the prediction of boundary-layer flows.

$$0 \leqslant z_E \leqslant 1: \quad -m_G = 0{\cdot}075(1-z_E),$$

$$1 < z_E: \quad -m_G = 0{\cdot}03z_E - 0{\cdot}02.$$

These relations imply a discontinuity at $z_E = 1$, a result of fitting 'best' straight lines to the data for $z_E < 1$ and $z_E > 1$.

In the following section a brief examination will be made of the sensitivity of the predictions to the entrainment function adopted.

For $z_E < 1$, an entrainment function deduced from the $G \sim \beta$ relation of Nash (1965) for equilibrium boundary layers is in qualitative agreement with the recommendation made above for $z_E < 1$. It is shown, however, that the entrainment function so derived is sensitive to small changes in the $G \sim \beta$ relation.

5. Comparison of the predictions of the present method with experimental data

5.1. *Methods of calculation*

The general prediction procedure involves the simultaneous solution of the differential equations derived in § 2 from the integral mass-conservation equation and the momentum integral equation. The required input is the variation of u_G with R_x and two initial conditions. In the case of boundary layers with $z_E < 1$, these initial conditions were taken as the values of R_m and z_E computed from the reported measured value of R_2 and H at the starting-point. For wall jets the initial values of z_E and R_m were deduced from the measured velocity profile at the starting-point using the least-squares-fitting method.

The quantities predicted were the values of R_2, H and s. In addition, for wall-jet flows the values of the more usual wall-jet variables $u_{\max}/u_G$ and $y_{\frac{1}{2}}/y_c$ were computed with the aid of the assumed velocity profile, equation (3.2.4). As well as this general procedure, calculations for flows with $z_E < 1$ have been carried out using measured values of R_2 as data, the integral mass-conservation equation only being solved. Thompson (1964) came to the conclusion that experimental values of R_2 provide the best basis for comparing the calculated with the measured shape-factor development. This, it was argued, allows some account to be taken of the three-dimensional character of most real flows. Whilst this *may* be true, in completely new circumstances two-dimensional conditions have to be assumed and the prediction of both R_2 and H is necessary.

For equilibrium flows an alternative method of calculation was also used. The value of z_E was taken as the mean of the values deduced from the experimental values of R_2 and H. The prediction procedure again reduces to the integration of a single differential equation. In this case, however, we have an analytical expression for the entrainment law, equation (4.4.3),

$$-m_G = H_1 s(1+\beta+\beta/H).$$

5.2. *Discussion of predictions for flows with* $z_E < 1$

In figures 19–26 are shown reported measured values of R_2 and H plotted against R_x. Also shown are experimental values of skin-friction coefficients s, the method by which these were obtained being noted on the relevant graphs. On each of

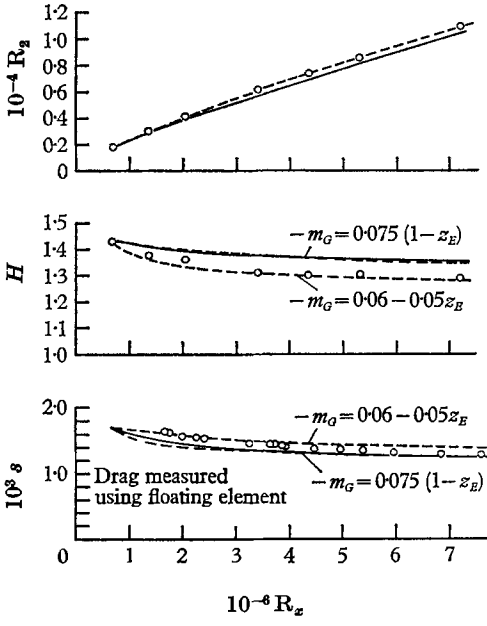

FIGURE 19

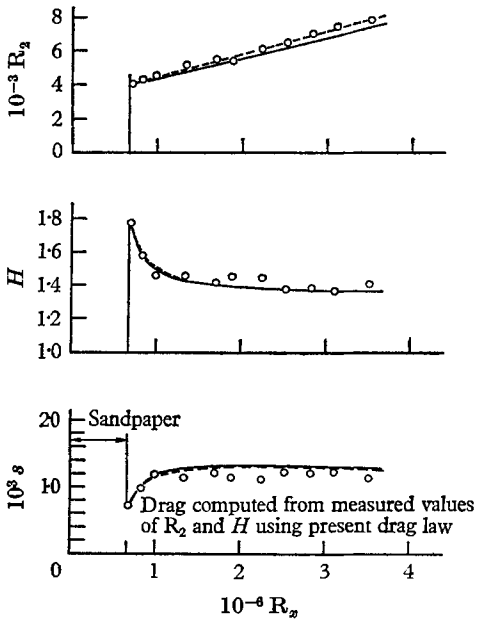

FIGURE 20

FIGURE 19. Comparison of predicted boundary-layer development with experimental data of Schultz–Grunow (1940). Flat-plate boundary layer.

FIGURE 20. Comparison of predicted boundary-layer development with experimental data of Klebanoff & Diehl (1952). Flat-plate boundary layer recovering from the effects of an upstream disturbance, $u_G = 35$ ft./sec.

these figures there appears a number of lines; those drawn full were obtained by the general prediction method (i.e. using as data only $u_G\{R_x\}$ and initial conditions). The chain-dashed lines on the H and s plots were computed using the dashed lines drawn through the plotted R_2 values as data. The additional lines appearing in the figures displaying data for equilibrium boundary layers were obtained assuming a constant value for z_E as outlined in § 5.1.

The following conclusions may be drawn from the comparisons:

(*a*) In the majority of the cases examined, agreement between the predictions and the experimental data is fairly good. Failure to predict R_2 accurately, however, leads to poor predictions of H and s.

(*b*) Predictions of H and s using measured R_2 values are generally better than those obtained when R_2 is computed simultaneously with H. The only exception to this generalization is the prediction of Clauser's second equilibrium boundary layer. The reason for the behaviour of this exceptional case is not yet known.

(c) The best predictions of the equilibrium boundary layers of Clauser are obtained when the appropriate constant value of z_E is assumed; this is hardly surprising since z_E and H are very strongly related to one another.

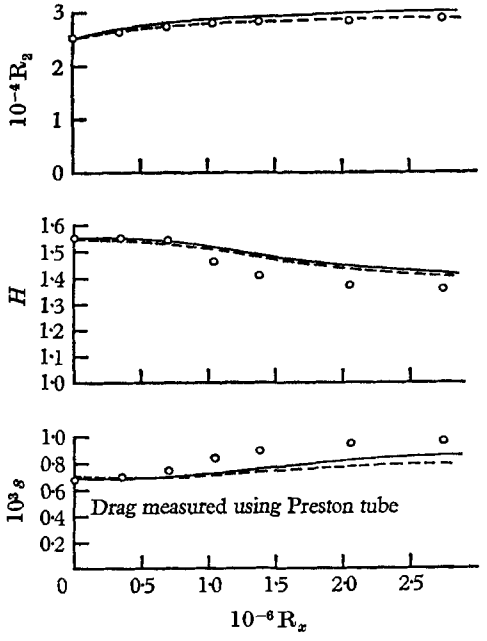

FIGURE 21

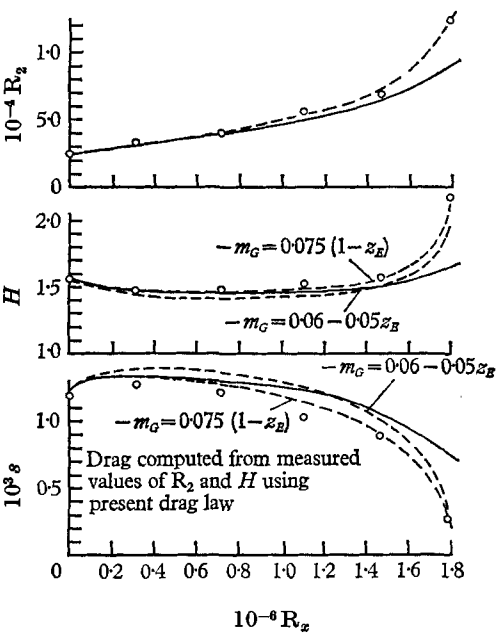

FIGURE 22

FIGURE 21. Comparison of predicted boundary-layer development with experimental data of Bradshaw & Ferriss (1965). Boundary layer recovering from the effects of an adverse pressure gradient.

FIGURE 22. Comparison of predicted boundary-layer development with experimental data of von Doenhoff & Tetervin (1943). Boundary layer on an aerofoil, *NACA* 65 (216) 222 (approx.), $R = 3{\cdot}64 \times 10^6$, $\alpha = 10{\cdot}1°$.

For the boundary layers of Schultz–Grunow (1940) and of von Doenhoff & Tetervin (1943) additional predictions of H and s were made using an entrainment equation differing from that recommended here. The equation used was that recommended by Spalding (1965)

$$-m_G = 0{\cdot}06 - 0{\cdot}05 z_E.$$

In the discussion in § 4.3 it was shown that this entrainment function is a better fit to the experimental data for the flat-plate boundary layer than is equation (4.3.2), the present recommendation. This view is supported by the graphs shown in figure 19, where it is seen that the prediction of Schultz–Grunow's boundary layer is considerably improved using this equation.

Figure 22, however, indicates that Spalding's entrainment equation leads to poorer predictions in the case of the flow reported by von Doenhoff & Tetervin than does the present authors' recommendation.

5.3. *Discussion of predictions of flows with* $z_E > 1$

Comparisons of measured with predicted wall-jet development are shown in figures 27–36. The data shown were reported by Kruka & Eskinazi (1953) and Nicoll (1965) and cover the following ranges of slot Reynolds numbers

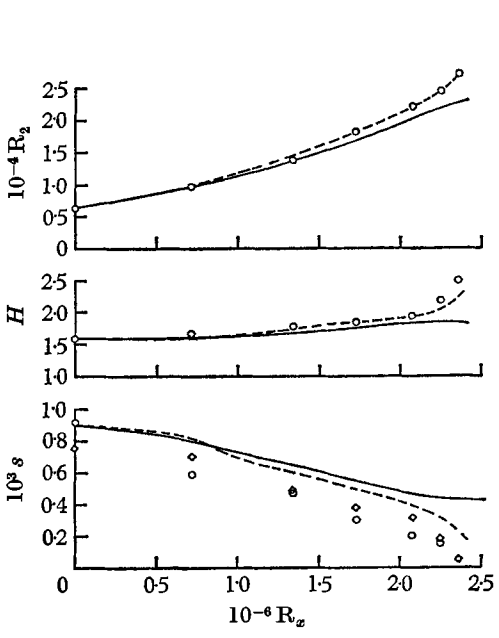

FIGURE 23

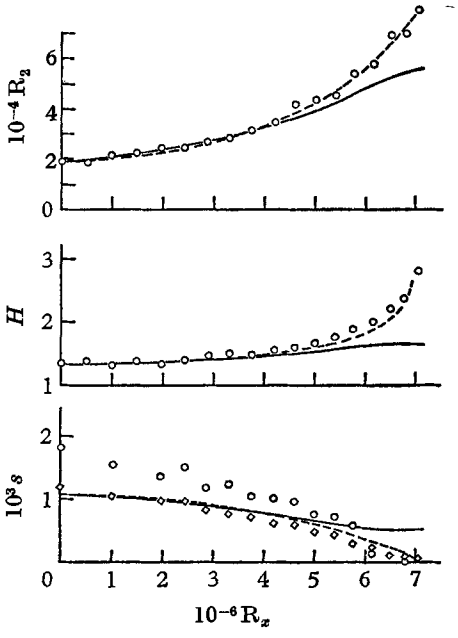

FIGURE 24

FIGURE 23. Comparison of predicted boundary-layer development with experimental data of Newman (1951). Boundary layer on a symmetrical rear-stalling aerofoil. ○, Drag obtained by extrapolating measured shear-stress profiles to wall. ◇, Drag obtained from velocity profiles by Clauser's method.

FIGURE 24. Comparison of predicted boundary-layer development with experimental data of Schubauer & Klebanoff (1951). Boundary layer on a convex wall with an adverse pressure gradient. ○, Drag obtained by extrapolating measured shear-stress profiles to wall. ◇, Drag obtained from velocity profiles by Clauser's method.

$R_c (\equiv u_c y_c/\nu)$ and velocity ratios $(u_c/u_{G,0})$,

$$3{,}000 \leqslant R_c \leqslant 24{,}000,$$

$$1{\cdot}55 \leqslant u_c/u_{G,0} \leqslant 18.$$

In general the predictions follow the experimental results quite closely and it may be concluded that the present method satisfactorily predicts wall-jet development over the range of pressure gradients and velocity ratios examined.

6. Conclusions

6.1. *Velocity profiles*

The velocity profile assumed in the present work, equation (3.2.4), appears to fit experimental velocity profiles adequately for the range

$$0{\cdot}5 < z_E < 5 \quad \text{(approx.)}.$$

At lower z_E the values of the shape factor, H, and the momentum thickness, δ_2, deduced from the least-squares-fitted profile differ significantly from the experi-

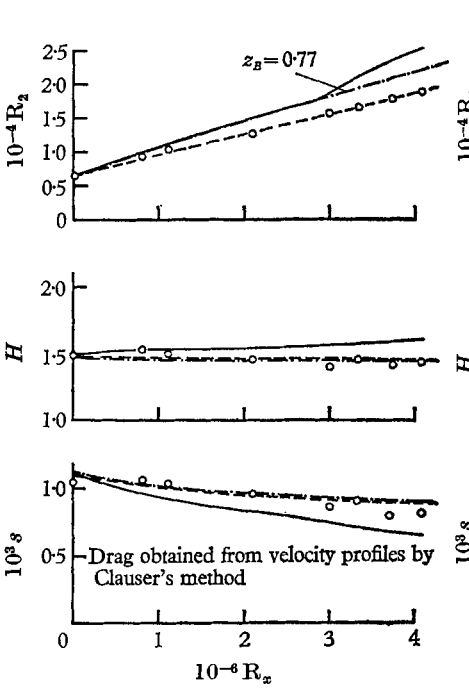

FIGURE 25

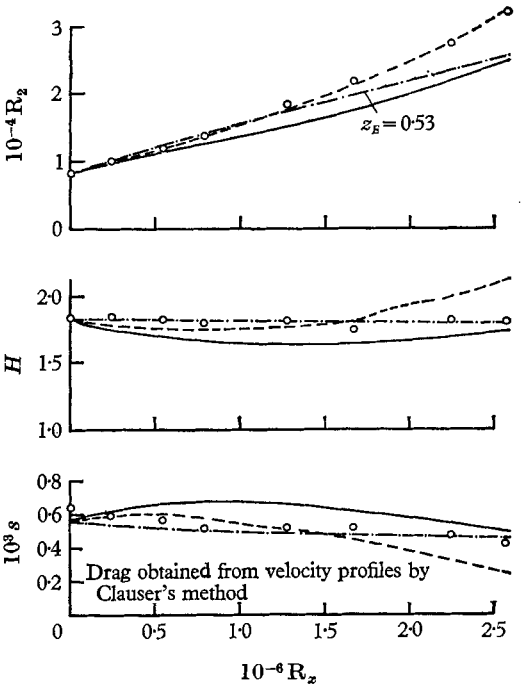

FIGURE 26

FIGURE 25. Comparison of predicted boundary-layer development with experimental data of Clauser (1954), pressure distribution 1. Equilibrium boundary layer with an adverse pressure gradient, $\beta \approx 1{\cdot}8$, $z_E \approx 0{\cdot}77$.

FIGURE 26. Comparison of predicted boundary-layer development with experimental data of Clauser (1954), pressure distribution 2. Equilibrium boundary layer with an adverse pressure gradient, $\beta \approx 8{\cdot}0$, $z_E \approx 0{\cdot}53$.

mental values. At higher z_E, the shape of the experimental profiles differs in a consistent manner from that of the assumed profile. The values of H, δ_2, $y_{\frac{1}{2}}$ and $u_{\max}$ obtained from the least-squares-fitted profile agree closely with the experimental values, although the value of $y_{\max}$ so obtained does not.

The drag law implicit in the assumed profile is an improvement over the Ludwieg–Tillmann drag law at high values of the shape factor H and has the advantage of being applicable to wall-jet flows.

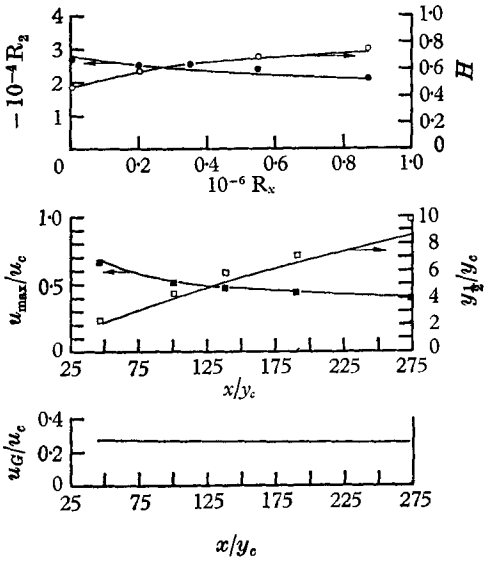

FIGURE 27

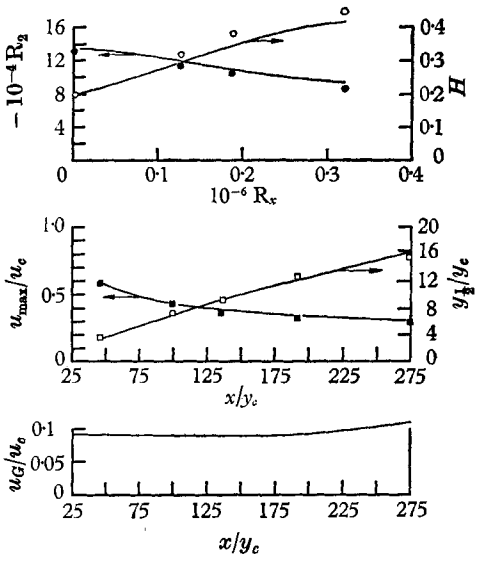

FIGURE 28

FIGURE 27. Comparison of predicted wall-jet development with experimental data of Kruka & Eskinazi (1963), run 1. $u_c/u_{G,0} = 3{\cdot}8$, $R_c = 1{\cdot}07 \times 10^4$. ●, R_2; ○, H; ■, u_{max}/u_c; □, $y_{\frac{1}{2}}/y_c$.

FIGURE 28. Comparison of predicted wall-jet development with experimental data of Kruka & Eskinazi (1963), run 2. $u_c/u_{G,0} = 10$, $R_c = 1{\cdot}31 \times 10^4$. Symbols as for figure 27.

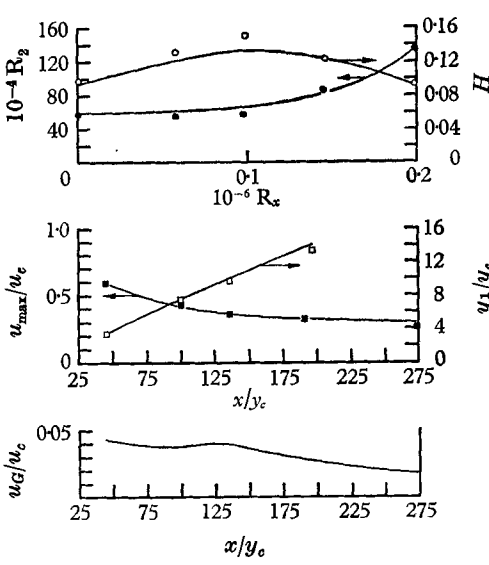

FIGURE 29

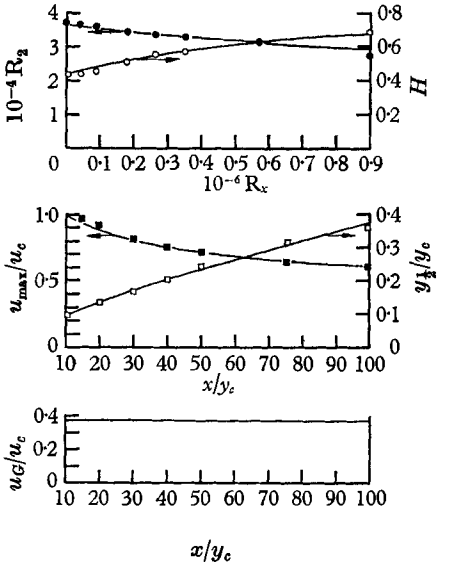

FIGURE 30

FIGURE 29. Comparison of predicted wall-jet development with experimental data of Kruka & Eskinazi (1963), run 3. $u_c/u_{G,0} = 18$, $R_c = 2{\cdot}63 \times 10^4$. Symbols as for figure 27.

FIGURE 30. Comparison of predicted wall-jet development with experimental data of Nicoll (1965), run 2. $u_c/u_{G,0} = 2{\cdot}71$, R $= 2{\cdot}37 \times 10^4$. Symbols as for figure 27.

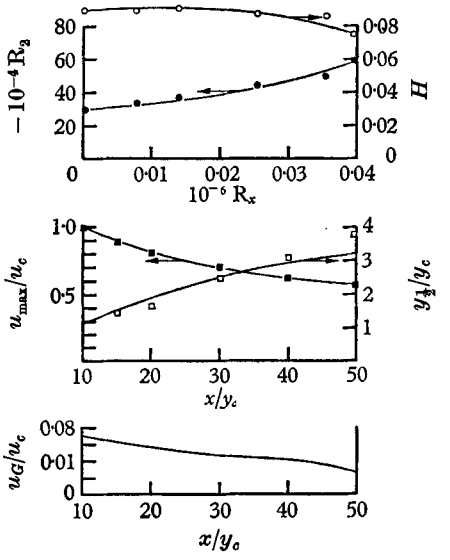

FIGURE 31

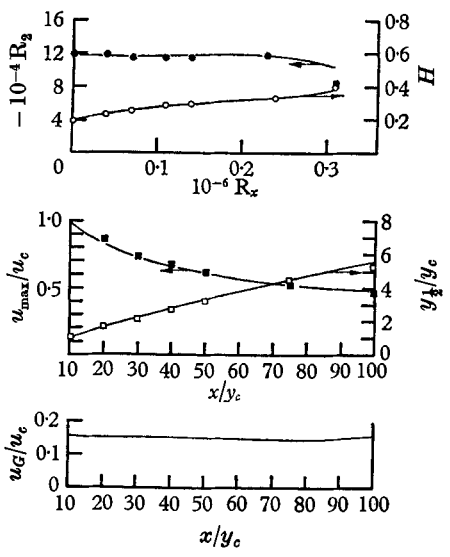

FIGURE 32

FIGURE 31. Comparison of predicted wall-jet development with experimental data of Nicoll (1965), run 3. $u_c/u_{G,0} = 13{\cdot}2$, $R_c = 2{\cdot}31 \times 10^4$. Symbols as for figure 27.

FIGURE 32. Comparison of predicted wall-jet development with experimental data of Nicoll (1965), run 4. $u_c/u_{G,0} = 6{\cdot}22$, $R_c = 2{\cdot}28 \times 10^4$. Symbols as for figure 27.

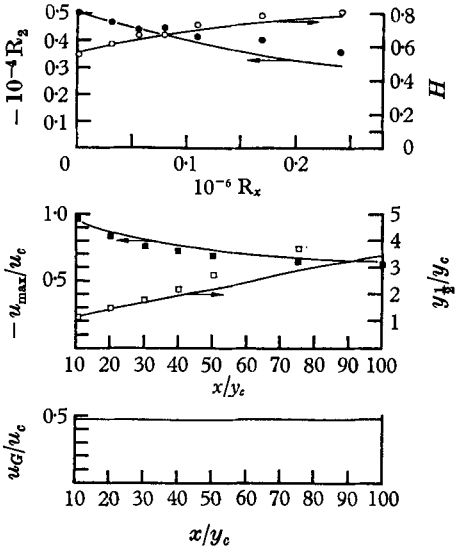

FIGURE 33

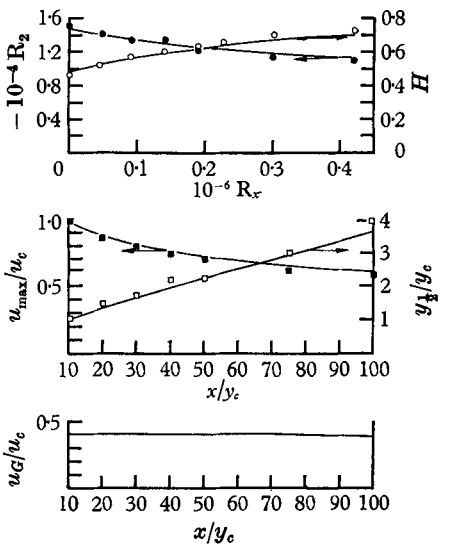

FIGURE 34

FIGURE 33. Comparison of predicted wall-jet development with experimental data of Nicoll (1965), run 5. $u_c/u_{G,0} = 2{\cdot}10$, $R_c = 5{\cdot}59 \times 10^3$. Symbols as for figure 27.

FIGURE 34. Comparison of predicted wall-jet development with experimental data of Nicoll (1965), run 7. $u_c/u_{G,0} = 2{\cdot}43$, $R_c = 1{\cdot}14 \times 10^4$. Symbols as for figure 27.

6.2. *Entrainment function*

Dimensionless entrainment rates are shown to correlate reasonably well with the parameter z_E. The following formulae fit the data as well as any and are the present authors' recommendations

$$0 \leqslant z_E \leqslant 1, \quad -m_G = 0{\cdot}075(1-z_E),$$

$$z_E > 1, \quad -m_G = 0{\cdot}03z_E - 0{\cdot}02.$$

The determination of entrainment requires both the specification of the outer edge of the boundary layer (for the determination of the flow within the boundary

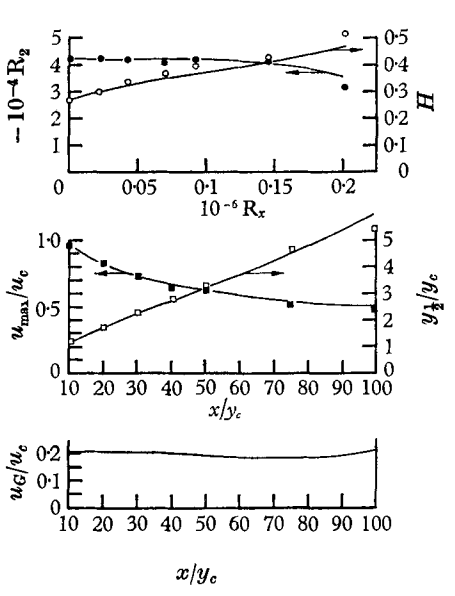

FIGURE 35

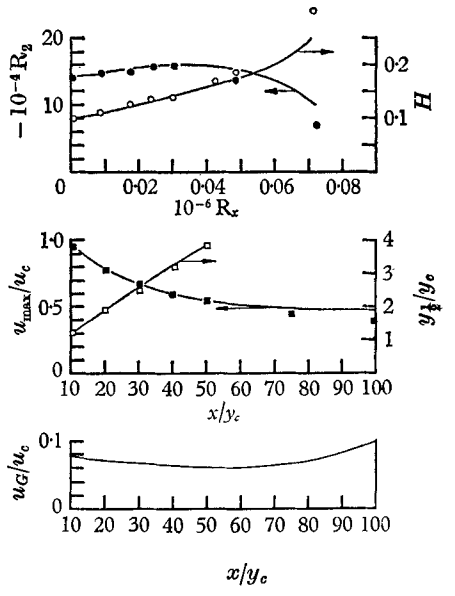

FIGURE 36

FIGURE 35. Comparison of predicted wall-jet development with experimental data of Nicoll (1965), run 9. $u_c/u_{G,0} = 4{\cdot}81$, $R_c = 1{\cdot}14 \times 10^4$. Symbols as for figure 27.

FIGURE 36. Comparison of predicted wall-jet development with experimental data of Nicoll (1965), run 10. $u_c/u_{G,0} = 12{\cdot}9$, $R_c = 1{\cdot}12 \times 10^4$. Symbols as for figure 27.

layer) and the differentiation of the flow so obtained. This gives rise to considerable scatter in the experimental entrainment rates and thus precludes the determination of any weaker dependence of entrainment on quantities other than z_E.

6.3. *Predictions*

Predictions have been made, using the recommended entrainment functions, of the shape factor H, momentum-thickness Reynolds number R_2 and drag coefficient s, and also, in the case of wall-jet flows, of the half-thickness $y_{\frac{1}{2}}$ and the velocity maximum u_{max}. The boundary-layer predictions are in reasonable agreement with experiment, except when separation conditions are approached.

Since the present form of the 'unified theory' applies only to two-dimensional flows, this failure may be due to lack of two-dimensionality in the reported separation experiments. Certainly the predictions based upon experimental values of R_2 are in good agreement with experiment, even when separation occurs. However, since the assumed velocity profile does not fit experimental profiles near separation conditions, the authors reserve their opinion as to the exact cause of the failure to predict separation.

The wall-jet predictions are good, both for zero pressure gradients and for adverse pressure gradients.

The authors would like to express their appreciation to Prof. D. B. Spalding for his help and advice in all stages of their work, which forms part of a programme of research, co-ordinated by Prof. Spalding, into turbulent flows near walls.

Thanks are also due to Mr P. Bradshaw, Prof. F. H. Clauser, Prof. S. Eskinazi, Dr V. Kruka and to Dr B. S. Stratford for making available to the authors unpublished details of their experimental work.

The support of the Ministry of Aviation (Contract no. PD/37/27) is gratefully acknowledged by W. B. Nicoll.

REFERENCES

Bradshaw, P. & Ferriss, D. H. 1965 The response of a retarded equilibrium turbulent boundary layer to the sudden removal of pressure gradient. *NPL Aero. Rep.* no. 1145.

Chi, S. W. 1962 Unpublished work at Imperial College.

Clauser, F. H. 1954 Turbulent boundary layers in adverse pressure gradients. *J. Aero. Sci.* **21**, 91.

Clauser, F. H. 1956 The turbulent boundary layer. *Advances in Applied Mechanics*, iv, no. 1. New York: Academic Press.

Coles, D. 1956 The law of the wake in the turbulent boundary layer. *J. Fluid Mech.* **1**, 191.

Coles, D. E. 1962 The turbulent boundary layer in a compressible fluid. *Rand Corp. Rep.* no. R–403–PR.

Doenhoff, A. E. von & Tetervin, N. 1943 Determination of general relations for the behaviour of turbulent boundary layers. *NACA TR*, no. 772.

Fage, A. 1938 Profile and skin-friction aerofoil drags. *Aero. Res. Counc. R. & M.* no. 1852.

Fage, A. & Falkner, V. M. 1930 An experimental determination of the intensity of friction on the surface of an aerofoil. *Aero. Res. Counc. R. & M.* no. 1315.

Gartshore, I. S. 1964 Jets and wall jets in uniform streaming flow. *McGill Univ., Mech. Eng. Res. Lab. Rep.* no. 64–4.

Head, M. R. 1960 Entrainment in the turbulent boundary layer. *Aero. Res. Counc. R. & M.* no. 3152.

Herring, H. J. & Norbury, J. F. 1963 Some experiments on equilibrium turbulent boundary layers in favourable pressure gradients. *Princeton Univ., Dept. Aerospace & Mech. Sci. FLD*, no. 15.

Hinze, J. O. 1959 *Turbulence*. New York: McGraw Hill.

Klebanoff, P. S. 1955 Characteristics of turbulence in a boundary layer with zero pressure gradient. *NACA Rep.* no. 1247.

Klebanoff, P. S. & Diehl, Z. W. 1952 Some features of artificially thickened fully developed turbulent boundary layers with zero pressure gradient. *NACA Rep.* no. 1110.

Kruka, V. & Eskinazi, S. 1964 The wall-jet in a moving stream. *J. Fluid Mech.* **20**, 555.

LUDWIEG, H. & TILLMANN, W. 1949 Untersuchungen über die Wandschubspannung in turbulenten Reibungsschichten. *Ing.-Arch.* **17**, 288. (Trans. 1950 Investigations of the wall shearing stress in turbulent boundary layers. *NACA TM*, no. 1285.)

MELLOR, G. J. & GIBSON, D. M. 1963. Equilibrium turbulent boundary layers. *Princeton Univ., Dept. Aerospace & Mech. Sci. FLD*, no. 13.

NASH, J. F. 1965 Turbulent-boundary-layer behaviour and the auxiliary equation. *AGARDograph*, no. 97, part 1, 245.

NEWMAN, B. G. 1951 Some contributions to the study of the turbulent boundary layer near separation. *Aust. Dept. Supply Rep.* no. ACA–53.

NICOLL, W. B. 1965 Wall jet velocity profiles and entrainment. *Imperial College, Mech. Eng. Dept. Rep.* no. IC/HRJ/23.

PATEL, R. P. & NEWMAN, B. G. 1961 Self-preserving, two-dimensional turbulent jets and wall jets in a moving stream. *McGill Univ., Mech. Eng. Res. Lab. Rep.* no. Ae 5.

REYNOLDS, W. C., KAYS, W. M. & KLINE, S. J. 1958 Heat transfer in the turbulent incompressible boundary layer. I Constant wall temperature. *NASA Memo*, no. 12–1–58 W.

SCHUBAUER, G. B. & KLEBANOFF, P. S. 1951 Investigation of separation of the turbulent boundary layer. *NACA Rep.* no. 1030.

SCHULTZ-GRUNOW, F. 1940 Neues Reibungswiderstandsgesetz für glatte Platten. *Luftfahrtforschung*, **17**, 239. (Trans. 1941 New frictional resistance law for smooth plates. *NACA TM* no. 986.)

SEBAN, R. A. & BACK, L. H. 1961 Velocity and temperature profiles in a wall jet. *Int. J. Heat & Mass Trans.* **3**, 255.

SMITH, D. W. & WALKER, J. H. 1959 Skin-friction measurements in incompressible flow. *NASA TR*, no. R–26.

SPALDING, D. B. 1964*a* A unified theory of friction, heat transfer and mass transfer in the turbulent boundary layer and wall jet. *Aero. Res. Counc. Rep.* no. 25,925.

SPALDING, D. B. 1964*b* A unified theory of friction, heat transfer and mass transfer in the turbulent boundary layer and wall jet. *Imperial College, Mech. Eng. Dep. Rep.* (Annotated version of previous reference.)

SPALDING, D. B. 1965 The kinetic-energy-deficit equation of the turbulent boundary layer. *AGARDograph*, no. 97, part 1, 191.

STRATFORD, B. S. 1959 An experimental flow with zero skin friction throughout its region of pressure rise. *J. Fluid Mech.* **5**, 17.

THOMPSON, B. G. J. 1964 A critical review of existing methods of calculating the turbulent boundary layer. *Aero. Res. Coun. Rep.* no. 26,109.

WIEGHARDT, K. 1944 Zum Reibungswiderstand rauher Platten. *ZWB KWI U & M*, 6612.